Guiding Electromagnetic Waves around Sharp Corners: Topologically Protected Photonic Transport in Metawaveguides

Tzuhsuan Ma, Alexander B. Khanikaev, S. Hossein Mousavi, and Gennady Shvets

Phys. Rev. Lett. **114**, 127401 — Published 23 March 2015

DOI: 10.1103/PhysRevLett.114.127401

Guiding Electromagnetic Waves Around Sharp Corners: Topologically Protected Photonic Transport in Meta-waveguides

Tzuhsuan Ma[1], Alexander B. Khanikaev[3,4], S. Hossein Mousavi[2], Gennady Shvets[1,*]

[1] Department of Physics, The University of Texas at Austin, Austin, Texas 78712, USA
[2] Department of Electrical Engineering, The University of Texas at Austin, Austin, Texas 78712, USA
[3] Department of Physics, Queens College of The City University of New York, Queens, New York 11367, USA and
[4]The Graduate Center of The City University of New York, New York, New York 10016, USA

*gena@physics.utexas.edu

The wave nature of radiation prevents its reflections-free propagation around sharp corners. We demonstrate that a simple photonic structure based on a periodic array of metallic cylinders attached to one of the two confining metal plates can emulate spin-orbit interaction through bianisotropy. Such meta-waveguide behaves as a photonic topological insulator with complete topological bandgap. An interface between two such structures with opposite signs of the bianisotropy supports topologically protected surface waves which can be guided without reflections along sharp bends of the interface.

Science thrives on analogies, and a considerable number of inventions and discoveries have been made by pursuing an unexpected connection to a very different field of inquiry. For example, photonic crystals (PhCs) have been referred to as "semiconductors of light" [1, 2] because of the far-reaching analogies between electron propagation in a crystal lattice and light propagation in a periodically modulated photonic environment. However, one aspect of electron behavior, its ***spin***, escaped emulation by photonic systems until recent [3, 4, 5, 6, 7] invention of photonic topological insulators (PTIs). The impetus for these developments in photonics came from the discovery of topologically nontrivial phases in condensed matter physics [8, 9, 10, 11, 12, 13] that give rise to topologically protected edge states immune to scattering. The realization of topologically protected transport in simple PhCs would circumvent a fundamental limitation imposed by the wave equation: inability of reflections-free light propagation along sharply bent pathway. Topologically protected electromagnetic states could be used for transporting photons without any scattering, potentially underpinning new revolutionary concepts in applied science and engineering.

Several approaches to making PTIs have been explored across the electromagnetic spectrum, including magnetic photonic crystals [14, 15, 16, 17, 18], cavity arrays [3], coupled ring resonators [4, 19], bi-anisotropic metamaterials [5], synthetic magnetic fields [6], and coupled helical fibers [7]. These approaches can be broadly separated into two groups: (a) those that rely on breaking the time-reversal symmetry (TRS) [14, 15, 16, 17, 18, 6], and (b) those that do not violate the TRS [4, 5]. We refer to the latter group of PTIs, which emulate the quantum spin Hall (SH) effect [9, 10, 11, 12, 13] and do not require an external magnetic field, as SH-PTIs. It was shown [5] that wave propagation in bianisotropic spin-degenerate metamaterials arranged into hexagonal PhCs can be described using the effective Kane-Mele Hamiltonian (KMH) introduced earlier [20, 21] to model graphene-like topological insulators with strong spin-orbit coupling (SOC). The macroscopic size [4, 19] and considerable complexity [5] of the proposed SH-PTIs rules them out as promising platforms for bending light on a wavelength spatial scale. One such greatly simplified photonic platform shown in Fig.1(a) is proposed in this Letter: a bi-anisotropic meta-waveguide (BMW) designed for emulating the KMH and providing photonic topological insulation.

The BMW is comprised of the parallel-plate metal waveguide filled with a periodically arranged hexagonal array of metallic cylinders connected to the top and/or bottom metal plates located at $z = \pm h_0/2$. The finite bianisotropy [22] is generated by a finite vacuum gap ($g_1 \neq 0$) between the rods and one of the metal plates as illustrated in Fig.1(c). The metal is modeled as a perfect electric conductor, i.e. the tangential component of the electric field vanishes at the metallic surface. In the analytically tractable case of $g_1 = 0$, the two (potentially degenerate) decoupled modes of interest of such PhC waveguide can be classified as TM (with non-vanishing field components E_z, H_x, and H_y) and TE (with non-vanishing E_x, E_y, H_x, H_y, and H_z) modes [23]. Under the Bloch ansatz, the following field decomposition is assumed by retaining just two lowest-order transverse modes:

$$H_z^{\mathrm{TE}}(\boldsymbol{r},t) = \sum_{n,\boldsymbol{k}_\perp} a_e^n(\boldsymbol{k}_\perp) h_z^{n,\boldsymbol{k}_\perp}(\boldsymbol{r}_\perp) \cos\left(\frac{\pi}{h_0} z\right) e^{i\boldsymbol{k}_\perp \cdot \boldsymbol{r}_\perp - i\omega_n(\boldsymbol{k}_\perp)t} + c.c. \tag{1}$$

$$E_z^{\mathrm{TM}}(\boldsymbol{r},t) = \sum_{n,\boldsymbol{k}_\perp} a_m^n(\boldsymbol{k}_\perp) e_z^{n,\boldsymbol{k}_\perp}(\boldsymbol{r}_\perp)\, e^{i\boldsymbol{k}_\perp \cdot \boldsymbol{r}_\perp - i\omega_n(\boldsymbol{k}_\perp)t} + c.c., \tag{2}$$

where $\boldsymbol{r}_\perp = (x, y)$, $\boldsymbol{k}_\perp = (k_x, k_y)$ are the Bloch wavenumbers inside the Brilloine zone (BZ), $h_z^{n,\boldsymbol{k}_\perp}(\boldsymbol{r}_\perp)$ and $e_z^{n,\boldsymbol{k}_\perp}(\boldsymbol{r}_\perp)$ are the normalized periodic field profiles such that $\int_{cell} dV \left(\epsilon \left|\boldsymbol{e}^{n,\boldsymbol{k}_\perp}\right|^2 + \mu_0 \left|\boldsymbol{h}^{n,\boldsymbol{k}_\perp}\right|^2\right) = 1$, and the $n = -,+$ index refers to lower (upper) propagation bands. Note that, by limiting the expansion basis and thereby constraining the z −dependence of the fields, the above ansatz is a crucial simplification which is needed to make further analytic progress. However, all numerical results shown in Figs.1-4 are obtained using first-principles electromagnetic simulations COMSOL Multiphysics® that are not subject to the reduced expansion basis approximation given by Eqs.(1-2).

The eigenfrequencies $\omega_n(\boldsymbol{k}_\perp)$ are doubly-degenerate for $\boldsymbol{k}_\perp = \pm \boldsymbol{e}_x 4\pi/3a_0$ corresponding to the $K(K')$ edges of the Brillouin zone shown in the inset to Fig.1(b). The hexagonal symmetry of the "photonic graphene" [24] lattice guarantees the appearance of the Dirac cone for the decoupled TE/TM modes. The field profiles of the two degenerate modes are shown in Fig.1(c). The photonic band structure plotted in Fig.1(b) shows the degenerate TE and TM Dirac cones overlapping at the K point of the Brillouin zone at the frequency $\omega_D = \omega_D^{\mathrm{TE}} = \omega_D^{\mathrm{TM}}$. For a given period a_0, the degeneracy between TE and TM modes' frequencies and group velocities $v_D \equiv \partial\omega/\partial k$ is obtained by the judicious choice of h_0 and the cylinders' diameter d_0. Such mode-degeneracy is essential [5] for establishing spin-like linear combinations of the

TE/TM modes which can be coupled to each other by a bi-anisotropic perturbation of the photonic structure.

Opening an air gap breaks the σ_z mirror symmetry and introduces the requisite bi-anisotropic response of the meta-waveguide [22] as schematically explained in Fig.1(a, right insets): the electric field in the gap between the cylinder and the plate $E_{x(y)}$ induces anti-symmetric currents $j_{x(y)}$ producing the net orthogonal magnetic moment $m_{y(x)}$, and vice versa. The photonic band structure (PBS) of the resulting bi-anisotropic crystal ($g_1 = g_0 \equiv 0.15a_0$) is shown in Fig.1(d), indicating that a complete photonic bandgap is formed in the $0.72 < \omega a_0/2\pi c < 0.77$ frequency range. As analytically demonstrated below, the finite rod-plate gap mimics the SOC in a graphene-like photonic structure, thereby turning the BMW shown in Fig.1 into a PTI as long as the lowest-order TE/TM modes are dominant.

The effective Hamiltonian for the photonic states of the BMW in the vicinity of the K point is constructed by combining two methodologies: (a) degenerate perturbation theory originally developed [15] for non-reciprocal photonic crystals supporting a doubly-degenerate TM mode, and (b) the classic Slater theory [25] describing the modification of the modes of an electromagnetic cavity by the perturbation of its boundaries (See Supplemental Material at [URL will be inserted by publisher] for detailed derivations). These two techniques are applied to a BMW perturbed by an asymmetric addition of a metal volume ("washer") shown in Fig.1(a, right inset) which is conceptually equivalent to the asymmetric gap as far as its bi-anisotropic response is concerned. The unperturbed basis for the perturbation theory at the K point consists of the TE/TM modes whose field profiles are shown in Fig.2. The modes' dispersion relations $\omega_{\pm}(\delta\boldsymbol{k}) = \omega_{e,m} \pm v_D|\delta\boldsymbol{k}|$ are linear [15] in $\delta\boldsymbol{k} \equiv \boldsymbol{k} - \boldsymbol{K}$ in the vicinity of the Dirac point, at which the frequencies of the TE/TM modes are $\omega_{e,m}$, respectively.

Finite $\delta\boldsymbol{k} \neq \boldsymbol{0}$ breaks the degeneracy for each mode and, for $\delta k > 0$, renders the upper (lower) band modes forward (backward) propagating as shown in Fig.2. We also observe that the basis eigenmodes become linearly polarized (LP) based on the average direction of its magnetic field: the forward/backward modes e_+/m_- are x-polarized while the backward/forward modes e_-/m_+ are y-polarized. The boundary perturbation couples the i'th and j'th basis modes with the normalized coupling coefficient given by $\Delta_{ij} = -\int_{\Delta V}\left(\boldsymbol{e}_i^* \cdot \boldsymbol{e}_j - \boldsymbol{h}_i^* \cdot \boldsymbol{h}_j\right) dV$, where ΔV is the volume displaced by the metal washer. Using a vector representation $\boldsymbol{a}_e = [a_{e_-}; a_{e_+}]$ and $\boldsymbol{a}_m = [a_{m_-}; a_{m_+}]$ [where $a_{e(m)\pm}$ is shorthand for $a_{e(m)}^{\pm}(\boldsymbol{K} + \delta\boldsymbol{k})$] for the complex-valued amplitudes of the expansion basis, we calculate the perturbed frequencies $\omega'(\delta\boldsymbol{k})$ by solving the following eigenvalue equation:

$$\begin{bmatrix} \omega_e(1 + \Delta_{ee})\hat{I} - v_D|\delta\boldsymbol{k}|\hat{\sigma}_z & -\omega_e\Delta_{em}\hat{\sigma}_y \\ -\omega_m\Delta_{em}\hat{\sigma}_y & \omega_m(1 + \Delta_{mm})\hat{I} - v_D|\delta\boldsymbol{k}|\hat{\sigma}_z \end{bmatrix} \begin{bmatrix} \boldsymbol{a}_e \\ \boldsymbol{a}_m \end{bmatrix} = \omega' \begin{bmatrix} \boldsymbol{a}_e \\ \boldsymbol{a}_m \end{bmatrix}, \tag{3}$$

where $\hat{\sigma}_x$, $\hat{\sigma}_y$, $\hat{\sigma}_z$ are the Pauli matrices, and $\hat{I}$ is a 2×2 unity matrix.

According to Eq.(3), the perturbation has two effects on the modes. First, the modes' frequencies $\omega_{e,m}$ are renormalized by the diagonal Δ_{ee}/Δ_{mm} terms. Second, the cross-coupling bianisotropic terms $\Delta_{em}(d_1, h_1; z_1) = \int_{\Delta V} \boldsymbol{h}_e^* \cdot \boldsymbol{h}_m \, dV = -\Delta_{em}(d_1, h_1; -z_1)$ satisfy the following selection rule that follows from the field profiles shown in Fig.2: they couple the TE/TM modes propagating in the opposite directions. The anti-symmetry of Δ_{em} with respect to z_1 follows from the eigenmodes' symmetry: $h_{e,x/y}(x, y, -z) = -h_{e,x/y}(x, y, z)$ and $h_{m,x/y}(x, y, -z) = +h_{m,x/y}(x, y, z)$.

The effective Hamiltonian $\mathcal{H}_K^{em}$ represented by the 4×4 matrix in the lhs of Eq.(3) can be transformed to $\mathcal{H}_K^{\uparrow\downarrow} = U\, \mathcal{H}_K^{em}\, U^{-1}$ by a unitary transformation from the LP basis $\mathbf{A}_K = [\boldsymbol{a}_e; \boldsymbol{a}_m]$ of TE/TM modes to a circularly polarized (CP) basis $\boldsymbol{\Psi}_K = U\mathbf{A}_K$ of spin states, where the transformation matrix U is given by the following Kronecker product:

$$U = \frac{1}{2}\begin{pmatrix} 1-\beta & 1+\beta \\ 1-\beta & -1-\beta \end{pmatrix} \otimes \begin{pmatrix} e^{-i\phi/2} & ie^{-i\phi/2} \\ -e^{i\phi/2} & ie^{i\phi/2} \end{pmatrix}, \tag{4}$$

where $2\omega_D = \omega_e + \omega_m$, $2\Delta\omega_D = \omega_e - \omega_m$, $2\omega_D' = \omega_e(1 + \Delta_{ee}) + \omega_m(1 + \Delta_{mm})$, $2\Delta\omega_D' = \omega_e(1 + \Delta_{ee}) - \omega_m(1 + \Delta_{mm})$, $\beta = \Delta\omega_D/2\omega_D$, and the phase ϕ is defined by $|\delta\boldsymbol{k}|e^{i\phi} \equiv \delta k_x + i\delta k_y$. It is possible to design the "dressed" frequencies $\omega_e' = \omega_e(1 + \Delta_{ee})$ and $\omega_m' = \omega_m(1 + \Delta_{mm})$ to be equal to each other, in which case the spin-degeneracy [5] condition $\Delta\omega_D' = 0$ is satisfied. The resulting eigenvalue equation $\mathcal{H}_K^{\uparrow\downarrow}\boldsymbol{\Psi}_K = \Omega\boldsymbol{\Psi}_K$ then assumes a block-diagonal form:

$$\begin{bmatrix} v_D\delta\boldsymbol{k}\cdot\hat{\boldsymbol{\sigma}} + \omega_D\Delta_{em}\hat{\sigma}_z & 0 \\ 0 & v_D\delta\boldsymbol{k}\cdot\hat{\boldsymbol{\sigma}} - \omega_D\Delta_{em}\hat{\sigma}_z \end{bmatrix}\begin{bmatrix} \boldsymbol{\psi}_K^{\uparrow} \\ \boldsymbol{\psi}_K^{\downarrow} \end{bmatrix} = \Omega\begin{bmatrix} \boldsymbol{\psi}_K^{\uparrow} \\ \boldsymbol{\psi}_K^{\downarrow} \end{bmatrix}. \tag{5}$$

where $\hat{\boldsymbol{\sigma}} = (\hat{\sigma}_x, \hat{\sigma}_y)$, and $\boldsymbol{\psi}_K^{\uparrow(\downarrow)} \equiv [\psi_K^{R,\uparrow(\downarrow)}; \psi_K^{L,\uparrow(\downarrow)}]$ are the spin-up (down) components of the $\boldsymbol{\Psi}_K \equiv [\boldsymbol{\psi}_K^{\uparrow}; \boldsymbol{\psi}_K^{\downarrow}]$ eigenvector, and $\Omega = \omega' - \omega_D'$ is the detuning from the "dressed" Dirac frequency ω_D'.

The physical meaning of the new spin-polarized CP photonic states ('R' for right and 'L' for left) is clarified by calculating $U^{-1}\boldsymbol{\Psi}_K$ to obtain the following expressions in the original TE/TM LP basis under the $\beta \ll 1$ assumption: $\boldsymbol{\Psi}_K^{R/L,\uparrow} = [1; \mp i;\ 1;\ \mp i]$ and $\boldsymbol{\Psi}_K^{R/L,\downarrow} = [1; \mp i;\ -1;\ \pm i]$. Therefore, the relative phase between TE and TM modes represents [5] the spin degree of freedom (DOF), and the handedness (i.e. the phase shift between the two LP components) represents the orbital DOF. By introducing Pauli matrices $\hat{s}$ that act on the spin components of $\boldsymbol{\Psi}_K$, Eq.(5) can be written in a more compact form as $\mathcal{H}_K^{\uparrow\downarrow} = v_D\hat{s}_0(\delta k_x\hat{\sigma}_x + \delta k_y\hat{\sigma}_y) + \omega_D\Delta_{em}\hat{s}_z\hat{\sigma}_z$, where $\hat{s}_0$ is a unity matrix, and the Kronecker product shorthand (e.g., $\hat{s}_0\hat{\sigma}_z \equiv \hat{s}_0 \otimes \hat{\sigma}_z$) is used.

Expanding the space of photonic states to include the vicinities of both K and K' points, i.e. by introducing the 8-component spinor $\mathbf{\Psi} = [\mathbf{\Psi}_K; \mathbf{\Psi}_{K'}]$, the combined 8×8 effective Hamiltonian matrix can be written (see the SM for details) as

$$\mathcal{H} = v_D\left(\delta k_x \hat{\tau}_z \hat{s}_0 \hat{\sigma}_x + \delta k_y \hat{\tau}_0 \hat{s}_0 \hat{\sigma}_y\right) + \omega_D \Delta_{em} \hat{\tau}_z \hat{s}_z \hat{\sigma}_z, \tag{6}$$

where $\hat{\tau}_z$ and $\hat{\tau}_0$ are the Pauli and identity matrices acting on the subspace combining the K and K' points of the BZ. Because Eq.(6) is identical to KMH [20], it defines the photonic modes that have the same topological nature as the electronic states in graphene with strong SOC described by the last term. Therefore, the BMW is an example of a SH-PTI that possesses a spectral bandgap $\Delta\omega_{gap} = 2\omega_D|\Delta_{em}|$ induced by the bianisotropy. An interface between two BMWs with opposite signs of Δ_{em} exemplified by Fig.3(a) is, therefore, expected to support two pairs [14, 5] of topologically protected surface waves (TPSW). This prediction is confirmed using first-principles COMSOL simulations of the PBS of the double-BMW plotted Fig.3(b), where four spin-locked surface photonic modes (one forward-propagating spin-up pair and another backward-propagating spin-down pair) are plotted with solid lines.

Several important properties of TPSWs can be observed from Fig.3. First, these are indeed surface modes because their energy density is tightly confined to the topological interface as shown in Fig.3(c). Second, the polarization state of TPSWs is spatially entangled [5] with the spin state. Specifically, from the directional flow of the Poynting flux plotted with arrows in Fig.3(c) inside the rod/plate gap, we observe that the spin-up and spin-down surface modes have opposite handedness: R/L for the spin up/down states. This essential feature enables directional excitation of TPSWs with a single rotating electric or magnetic dipole. By placing an L-polarized dipole inside the air gap adjacent to the interface, backward-propagating spin-down TPSW is excited as shown in Fig.3(d). In contrast, directional excitation of topologically trivial surface waves requires a series of phase-shifted dipoles placed along the propagation directions [26], thereby increasing the device size.

Third, the gapless crossing of the surface modes corresponding to different spin states shown in Fig.3(b) indicates the lack of spin flipping. The spin conservation results in a topologically protected spin-polarized transport of TPSWs: their backscattering is expected to be suppressed even in the presence of various classes of structural perturbations (e.g., the variation of the gap size g_1 or gap position $z_1 = \pm h_0/2$) that preserve spin-degeneracy. Below we concentrate on a specific type of imperfection: a sharp bend of the interface shown in Fig.3(d). Because spin-degeneracy is maintained by such imperfections, we can expect that it should be possible to direct the flow of TPSWs along the bend without reflections. The results of a COMSOL simulation are shown in Fig.3(d), where we have investigated the transmission of a spin-polarized TPSW launched from the upper-right corner of a zigzag interface between two BMWs with opposite bianisotropy coefficients Δ_{em}. High broadband transmission of TPSWs, such that $T(\omega) > 0.9$ is achieved for 98% of the entire bandgap, is observed, indicating that two $120°$ turns of the wave along the correspondingly bent topological interface are accomplished with negligible reflection. Although the demonstrated topological protection is conceptually understood from our analytic theory that relies on the limited basis expansion given by Eqs.(1-2), the actual results shown in Fig.3 are obtained using first-principles electromagnetic simulations.

The unusual nature of such reflection-free propagation of an electromagnetic wave along a sharply curved interface can be appreciated by comparing it with the case of a standard (topologically trivial) interface between two photonic crystals with overlapping photonic bandgaps. We make such a comparison by considering an interface between two topologically-trivial photonic crystals (PhCs) shown in Fig.4(a). Each PhC consists of a hexagonal array of identical semi-circular metal rods attached to two metallic plates for vertical confinement. The interface between these PhCs is introduced by changing the orientation of the rods. The two PhCs possess identical gapped spectra shown in Fig.4(b). Different surface terminations of the PhCs form an interface supporting topologically trivial surface waves (TTSWs) [27] inside the bandgap. The propagation band $\omega_{TM}^{TTSW}(k_x)$ of the TTSW shown by the blue lines in Fig.4(b) was numerically calculated for the TM polarization. Any wavelength-scale perturbation of the interface (e.g., change in the rod's size or orientation), including a sharp bending of the interface, can induce reflections by scattering the forward-moving TTSW into its backward-moving counterpart.

One such zigzag propagation path corresponding to two $120°$ bends of the domain wall is shown in Fig.4(c). The transmission $T(\omega)$ of a TTSW launched by a point dipole placed in the upper-right corner of the simulation domain was numerically calculated for a range of frequencies spanning the entire bandgap of the interface-forming PhCs. The plot of $T(\omega)$ in Fig.4(d) exhibits two sharp 100% transmission peaks within the bandgap region. These transmission peaks are related to the phenomenon of resonant tunneling [28] through the cavity formed by the middle portion ("cavity") of the zigzag. Their spectral positions, often referred to as Fabry-Perot resonances, are determined by the length of the cavity. Backscattering is essential for the formation of Fabry-Perot resonances because, at peak transmission, TTSWs undergo multiple bounces inside the cavity. However, for all other frequencies inside the bandgap the transmission is very small. According to Fig.4(d), $T(\omega) > 0.9$ is achieved for just 5.6% of the entire bandgap. While it has been recently demonstrated [29] that it may be possible to reduce broadband wave reflections from PhC waveguides that are bent by as much as 90° by carefully designing the geometry of the bends, the general conclusion holds: complete elimination of reflections is only possible at Fabry-Perot resonances. This result should be contrasted with near-perfect transmission of TPSWs over the entire bandgap through an identical sequence of two bends of the mode-guiding interface shown in Fig.3(d).

In conclusion, a simple design of a topological photonic insulator emulating the Kane-Mele Hamiltonian with tunable spin-orbit interaction – a bi-anisotropic meta-waveguide (BMW) – has been introduced. Unlike earlier metamaterials-based designs, BMWs are non-resonant photonic structures that do not suffer from high Ohmic losses and could be potentially scaled to infrared optical frequencies. Domain walls between BMWs with reversed bianisotropy coefficient support topologically protected surface waves (TPSWs) that are formally described as photonic states with a conserved spin-like degree of freedom propagating in the direction prescribed by the sign of the spin. While the standard scalar wave equation in general prohibits reflectionless propagation of electromagnetic waves along the paths that are non-smooth on the wavelength spatial scale, the multi-component polarization state of TPSWs enables their guiding along sharply curved interfaces with negligible reflection as confirmed by our first-principles electromagnetic simulations. This unique functionality makes BMWs a promising platform for developing various applications in photonics and electromagnetics that benefit from compact and reflectionless routing of electromagnetic energy. This work was supported by the National Science Foundation (NSF) Awards DMR-1120923 and PHY-1415547.

References

1. Yablonovitch, E., Inhibited Spontaneous Emission in Solid-State Physics and Electronics. *Phys. Rev. Lett.* **58**, 2059-2062 (1987).

2. John, S., Strong localization of photons in certain disordered dielectric superlattices. *Phys. Rev. Lett.* **58**, 2486-2489 (1987).

3. Umucalılar, R. & Carusotto, I., Artificial gauge field for photons in coupled cavity arrays. *Physical Review A* **84** (4), 043804 (2011).

4. Hafezi, M., Demler, E. A., Lukin, M. D. & Taylor, J. M., Robust optical delay lines with topological protection. *Nature Physics* **7** (11), 907-912 (2011).

5. Khanikaev, A. B. *et al.*, Photonic topological insulators. *Nature Materials* **12** (3), 233-239 (2013).

6. Fang, K., Yu, Z. & Fan, S., Realizing effective magnetic field for photons by controlling the phase of dynamic modulation. *Nature Photonics* **6** (11), 782-787 (2012).

7. Rechtsman, M. C. *et al.*, Photonic Floquet topological insulators. *Nature* **496** (7444), 196-200 (2013).

8. Klitzing, K. v., Dorda, G. & Pepper, M., New method for high-accuracy determination of the fine-structure constant based on quantized Hall resistance. *Physical Review Letters* **45** (6), 494 (1980).

9. Bernevig, B. A., Hughes, T. L. & Zhang, S.-C., Quantum spin Hall effect and topological phase transition in HgTe quantum wells. *Science* **314**, 1757--1761 (2006).

10. König, M. *et al.*, Quantum spin Hall insulator state in HgTe quantum wells. *Science* **318** (5851), 766-770 (2007).

11. Hsieh, D. *et al.*, A topological Dirac insulator in a quantum spin Hall phase. *Nature* **452** (7190), 970-

974 (2008).

12. Xia, Y. *et al.*, Observation of a large-gap topological-insulator class with a single Dirac cone on the surface. *Nature Physics* **5** (6), 398-402 (2009).

13. Zhang, H. *et al.*, Topological insulators in Bi2Se3, Bi2Te3 and Sb2Te3 with a single Dirac cone on the surface. *Nature Physics* **5** (6), 438-442 (2009).

14. Haldane, F. & Raghu, S., Possible realization of directional optical waveguides in photonic crystals with broken time-reversal symmetry. *Phys. Rev. Lett.* **100**, 013904 (2008).

15. Raghu, S. & Haldane, F. D. M., Analogs of quantum-Hall-effect edge states in photonic crystals. *Phys. Rev. A* **78**, 033834 (2008).

16. Wang, Z., Chong, Y., Joannopoulos, J. & Soljačić, M., Reflection-free one-way edge modes in a gyromagnetic photonic crystal. *Phys. Rev. Lett.* **100**, 13905 (2008).

17. Wang, Z., Chong, Y., Joannopoulos, J. D. & Soljačić, M., Observation of unidirectional backscattering-immune topological electromagnetic states. *Nature* **461**, 772-775 (2009).

18. Poo, Y., Wu, R., Lin, Z., Yang, Y. & Chan, C. T., Experimental Realization of Self-Guiding Unidirectional Electromagnetic Edge States. *Phys. Rev. Lett.* **106**, 093903 (2011).

19. Hafezi, M., Mittal, S., Fan, J., Migdall, A. & Taylor, J. M., Imaging topological edge states in silicon photonics. *Nature Photonics* **7**, 1001–1005 (2013).

20. Kane, C. L. & Mele, E. J., Quantum Spin Hall Effect in Graphene. *Phys. Rev. Lett.* **95**, 226801 (2005).

21. Bernevig, B. A. & Zhang, S.-C., Quantum Spin Hall Effect. *Phys. Rev. Lett.* **96**, 106802 (2006).

22. Serdyukov, A. N., Semchenko, I. V., Tretyakov, S. A. & Sihvola, A., *Electromagnetics of bi-anisotropic materials: Theory and applications* (Gordon and Breach Science Publishers, Amsterdam, 2001).

23. Sakoda, K., *Optical Properties of Photonic Crystals* (Springer, Berlin, 2001).

24. Szameit, A., Rechtsman, M. C., Bahat-Treidel, O. & Segev, M., PT-symmetry in honeycomb photonic lattices. *Phys. Rev. A* **84**, 021806(R) (2011).

25. Slater, J. C., Microwave Electronics. *Rev. Mod. Phys.* **18** (4), 441-512 (1946).

26. Krasnok, A. E. *et al.*, Optical nanoantennas. *Physics-Uspekhi* **56** (6), 539 (2013).

27. Meade, R. D., Brommer, K. D., Rappe, A. M. & Joannopoulos, J., Electromagnetic Bloch waves at the surface of a photonic crystal. *Physical Review B* **44** (19), 10961 (1991).

28. Fan, S., Villeneuve, P. R., Joannopoulos, J. D. & Haus, H., Channel drop tunneling through localized states. *Physical Review Letters* **80** (5), 960 (1998).

29. Mekis, A. *et al.*, High transmission through sharp bends in photonic crystal waveguides. *Physical Review Letters* **77** (18), 3787 (1996).

30. Tai, C.-T., On the eigenfunction expansion of dyadic Green's functions. *Proceedings of the IEEE* **61** (4), 480-481 (1973).

31. Collin, R. E., Antennas, I. & Society, P., *Field theory of guided waves* (IEEE Press, 1991).

32. Mong, R. S. & Shivamoggi, V., Edge states and the bulk-boundary correspondence in Dirac Hamiltonians. *Physical Review B* **83** (12), 125109 (2011).

33. Simon, B., Holonomy, the quantum adiabatic theorem, and Berry's phase. *Physical Review Letters* **51** (24), 2167 (1983).

34. Sheng, D., Weng, Z., Sheng, L. & Haldane, F., Quantum spin-Hall effect and topologically invariant Chern numbers. *Physical review letters* **97** (3), 036808 (2006).

35. Thouless, D., Kohmoto, M., Nightingale, M. & Den Nijs, M., Quantized Hall conductance in a two-dimensional periodic potential. *Physical Review Letters* **49** (6), 405 (1982).

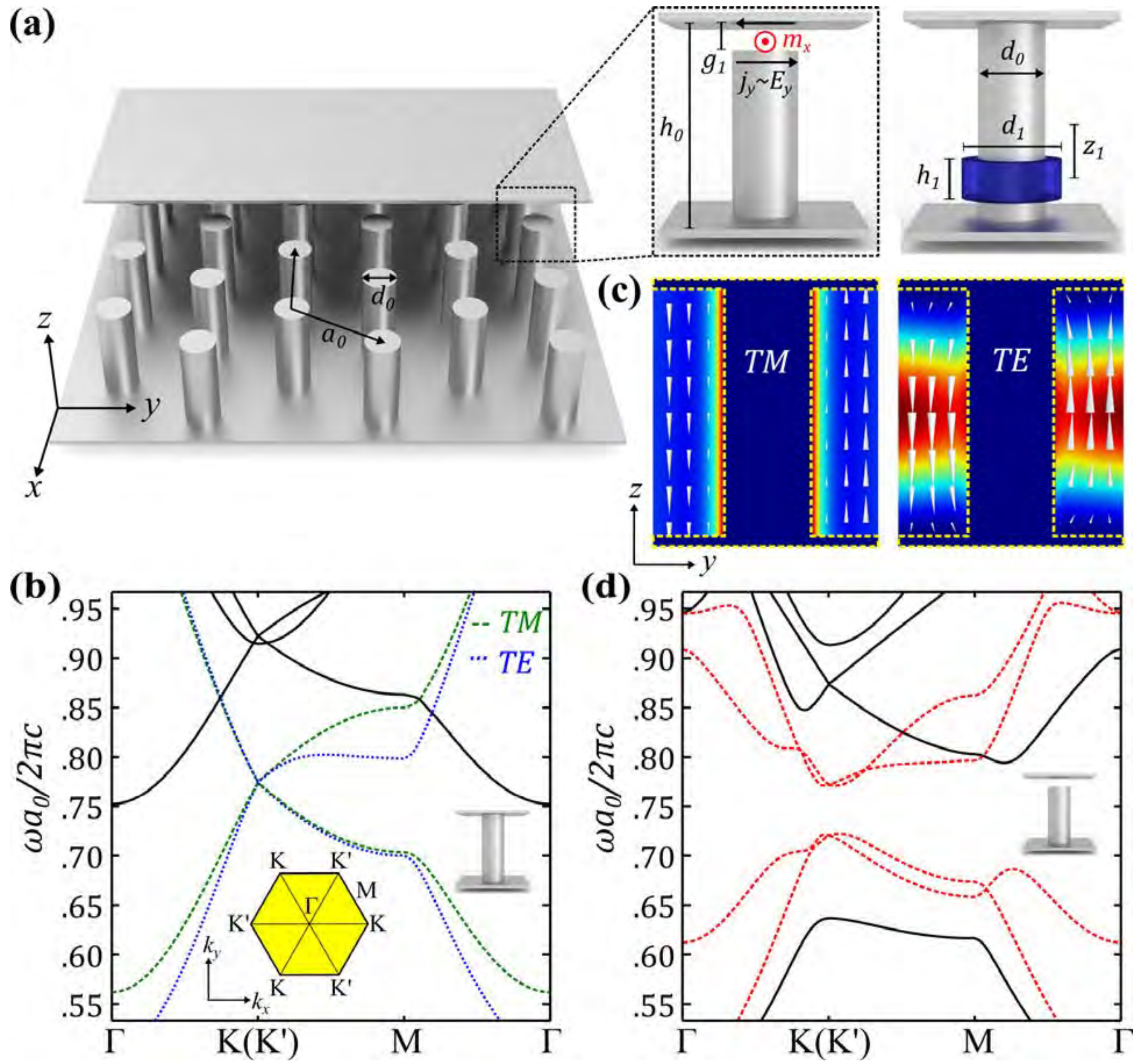

Figure 1: Bi-anisotropic meta-waveguide (BMW) as a photonic topological insulator. (a) Schematic of the BMW. Part of the top metal plate is removed to reveal the "bed-of-nails" structure below. The enlarged regions on the right illustrate the origin of the bi-anisotropic response. Right inset: an equivalent way to produce bianisotropy by adding an asymmetrically placed metallic volume ("washer") around the rod. **(b)** Photonic band structure (PBS) of spin-degenerate meta-waveguide ( ) with TE and TM modes forming doubly degenerate Dirac cones at points. **(c)** Field profiles of the degenerate TE and TM mode at the point. Colors: energy density. Arrows: electric field for the TM mode, and magnetic field for the TE mode. Yellow dashed line: metallic border. **(d)** PBS with the bandgap induced by the bianisotropy of the meta-waveguide ( ). Dashed lines in (b,d): TE/TM bands of interest. BMW parameters: , ,

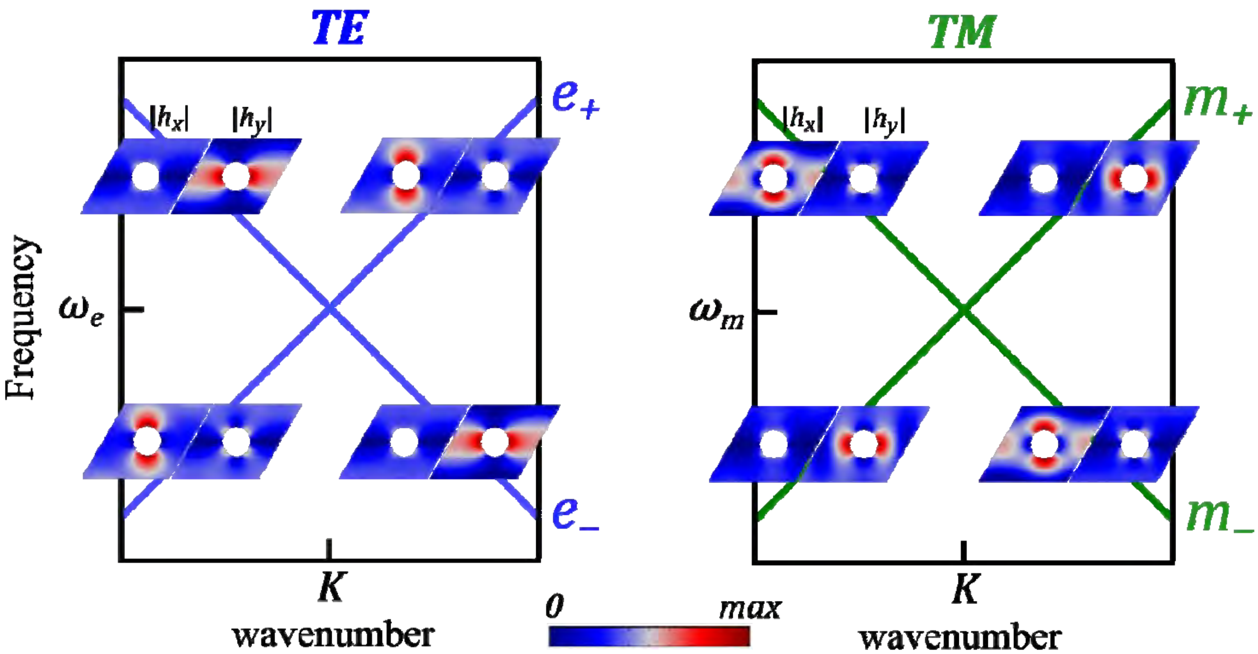

Figure 2: Dirac dispersion of the dipolar TE and dipolar TM modes in the vicinity of the point. The in-plane magnetic field profiles (on the left and on the right) are overlaid atop the band structure to show the dominant component of the magnetic field. The positive- and negative-group-velocity bands are labeled with ' ' and ' ' sign.

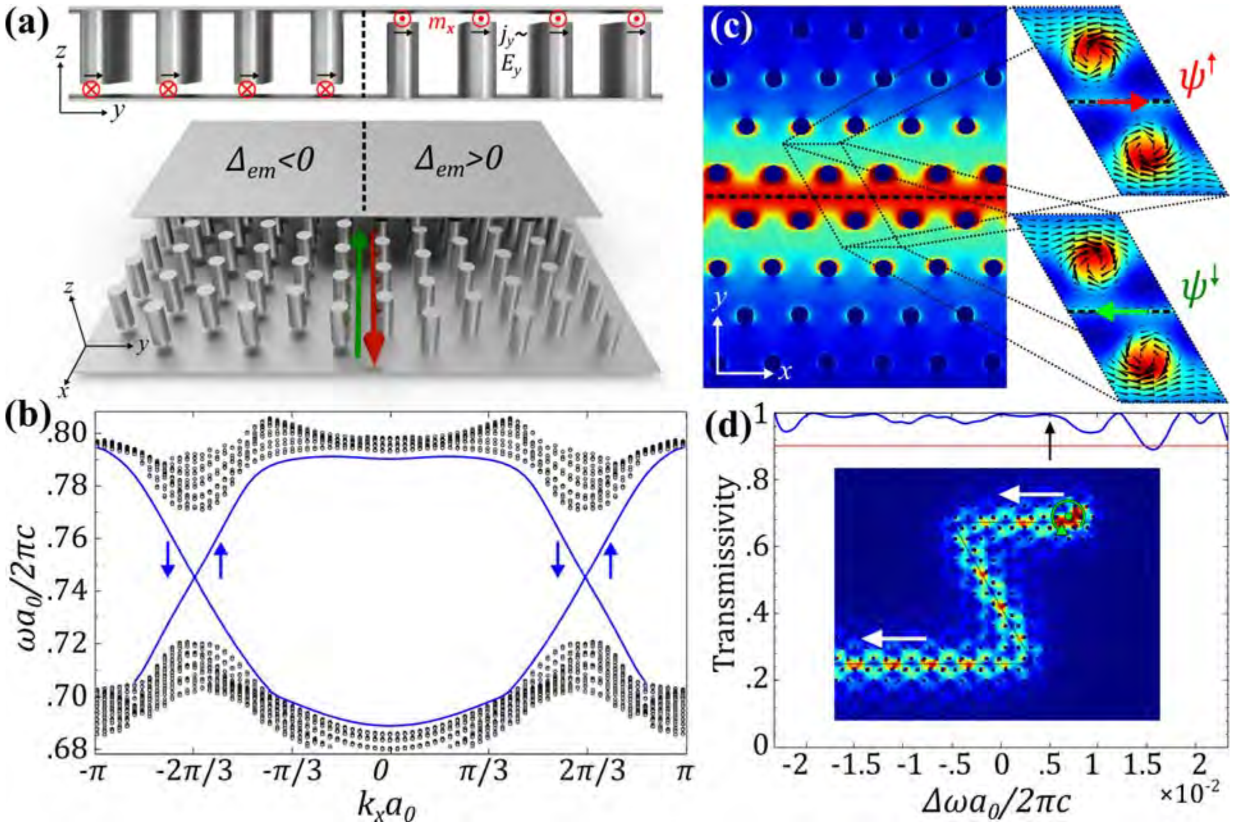

Figure 3: Propagation of topologically protected surface waves (TPSWs) along the interface between two topologically-nontrivial BMWs (a) Side and top views of the topologically-nontrivial interface (dashed line) between two BMWs introduced in Fig.1. **(b)** 1D PBS of a super cell (single cell along x-direction, 30 cells on each side of the interface) of the hybridized TE/TM modes. Black circles: bulk modes, blue lines: TPSW, arrows: spin state. **(c)** Color: energy density; arrows: Poynting flux of a TPSW at the frequency indicated by a black arrow in (d). **(d)** Transmission spectrum through the zigzag path, where is the detuning from the bandgap center at . Spin-down TPSWs are excited by placing an -polarized electric dipole between the rod and metal plate in the upper right corner. Red line: ; BMW parameters: same as in Fig. 1.

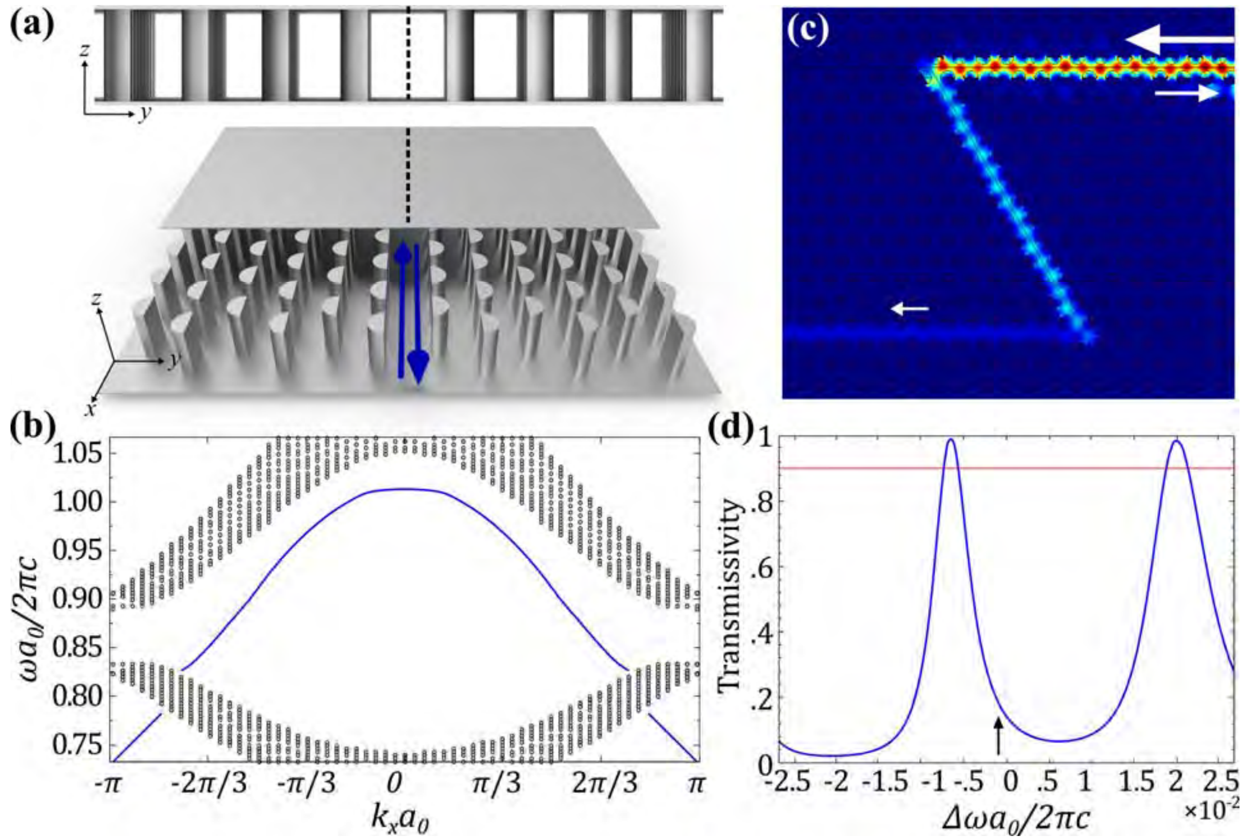

Figure 4: Propagation of surface waves along the interface between two topologically-trivial PhCs. (a) Side and top views of the two PhCs and their interface. Semi-circular metal rods arranged in a hexagonal pattern connect the two metal plates. **(b)** 1D PBS of a super cell (a single unit cell along x-axis, 30 unit cells on each side of the interface along y-axis) for TM modes. Black circles: bulk modes, blue lines: topologically trivial surface waves (TTSW). **(c)** Energy density of a TTSW with frequency indicated with black arrow in (d). **(d)** Transmission spectrum through the zigzag route, where spans the entire bandgap and corresponds to bandgap center at . Red line: . Structure parameters: , .